Accepted Manuscript

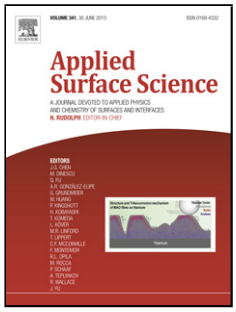

Title: Surfactant free controllable synthesis of 2D – 1D ZnO hierarchical nanostructure and its gas sensing properties

Authors: R. Sankar Ganesh, Ganesh Kumar Mani, R. Elayaraja, E. Durgadevi, M. Navaneethan, S. Ponnusamy, K. Tsuchiya, C. Muthamizhchelvan, Y. Hayakawa

PII: S0169-4332(18)30574-9
DOI: https://doi.org/10.1016/j.apsusc.2018.02.213
Reference: APSUSC 38671

To appear in: *APSUSC*

Received date: 8-9-2017
Revised date: 19-2-2018
Accepted date: 21-2-2018

Please cite this article as: R.Sankar Ganesh, Ganesh Kumar Mani, R.Elayaraja, E.Durgadevi, M.Navaneethan, S.Ponnusamy, K.Tsuchiya, C.Muthamizhchelvan, Y.Hayakawa, Surfactant free controllable synthesis of 2D – 1D ZnO hierarchical nanostructure and its gas sensing properties, Applied Surface Science https://doi.org/10.1016/j.apsusc.2018.02.213

Surfactant free controllable synthesis of 2D – 1D ZnO hierarchical nanostructure and its gas sensing properties

R. Sankar Ganesh [a, b, c], Ganesh Kumar Mani [d], R. Elayaraja [e], E. Durgadevi [c], M. Navaneethan [a, *], S. Ponnusamy [a, *], K. Tsuchiya [d], C. Muthamizhchelvan [a], Y. Hayakawa [c, *]

[a] *Center for Materials Science and Nano Devices, Department of Nanotechnology, SRM University, Kattankulathur, Kancheepuram 603203, Tamil Nadu, India.*

[b] *Graduate School of Science and Technology, Shizuoka University, 3-5-1 Johoku, Naka-ku, Hamamatsu, Shizuoka 432-8011, Japan*

[c] *Research Institute of Electronics, Shizuoka University, 3-5-1 Johoku, Naka-ku, Hamamatsu, Shizuoka 432-8011, Japan.*

[d] *Department of Precision Engineering, Micro/Nano Technology Center, Tokai University, Shonan Campus Hiratsuka, Kanagawa 259-1292, Japan*

[e] *Department of pharmacy, Annamalai University, Chidambaram, Tamil Nadu, India.*

*Corresponding authors. *E-mail address:* royhaya@ipc.shizuoka.ac.jp (Y. Hayakawa), m.navaneethan@gmail.com (M. Navaneethan), suruponnus@gmail.com (S. Ponnusamy),

Graphical abstract

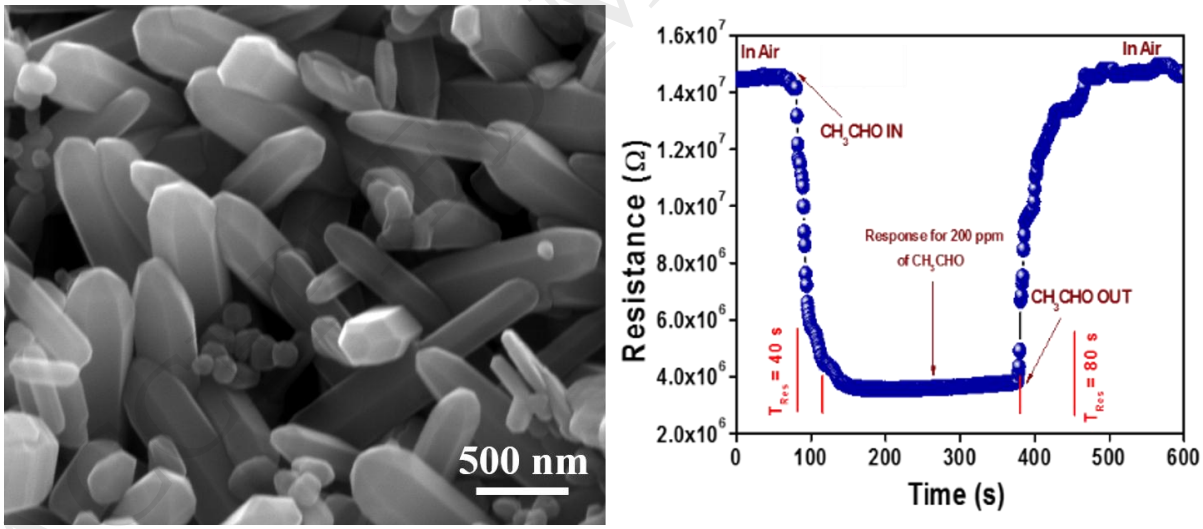

Highlights

- ZnO nanostructures synthesized without any template and capping agents.

- ZnO nanorods showed higher gas response towards acetaldehyde.

- Faster response and recovery times of 40 and 80 s towards 200 ppm of acetaldehyde.

Abstract

ZnO nanosheets, nanoflower, and nanorods were successfully synthesized without using any capping agent or surfactant by hydrothermal method. ZnO nanoparticle transformed into 2D – nanosheet and 1D nanorods with the increase of precursor concentration. The results clearly indicated that the molar ratio of Zn^{2+}/OH^- strongly influenced on the formation of hierarchical nanorods and nanosheet. FESEM and TEM images showed that the different morphologies such as nanoparticle, nanosheets and nanorods were obtained by varying the concentration of NaOH. HRTEM confirmed that the ZnO nanorods and nanosheets were well crystalline. ZnO showed higher response (S=92) towards acetaldehyde compared with other gases. It also showed faster response and recovery times of 40 and 80 s towards 200 ppm of acetaldehyde, respectively.

Keywords: Hierarchical nanostructures, Raman spectra, Nanosheet, Nanorod, Nanoparticle, Gas sensor

1. Introduction

Recent days researchers fascinated in finding way to identify advanced techniques concerning about food quality and environment monitoring for healthy life. Continuous gas monitoring provides flexible approach in a cost effective way to monitor the environment, industrial gas leakages and food quality too [1,2]. In this row, acetaldehyde (CH_3CHO) is recognized as carcinogenic and toxic and hence it must to be monitored continuously. The time weighted average (TWA) threshold is 100 ppm for 8 hours workday or short time exposure of 150 ppm for 15 mins leads to several health issues in human bodies. Moreover, recently wider and wider interest is rising in correlation in acetaldehyde concentration in human exhaled breath with various disease diagnosis. ZnO nanostructures have been investigated extensively because of their excellent optical and electrical properties compared to the bulk material. ZnO

is an important II – VI semiconductor material with direct bandgap 3.37 eV and high exciton binding energy 60 meV [3]. ZnO nanostructures have applications in several fields such as transparent electrodes, light emitting diodes, sensors etc [4]. It is well known that among the wide band gap semiconductor materials, ZnO shows the richest range of morphologies which simualted researchers to work on it [5]. Especially hierarchical nanostructures have been constructed by lower dimensional nanocrystals because their properties like high mobility, specific surface area and agglomeration configuration opened wide range of application such as photocatalysis, gas sensing, photoanode in dye sensitized solar cell, and blood vessels [6]. Various synthetic methodologies have been evolved for the synthesis of ZnO hierarchical architectures like chemical vapor condensation, arc discharge, hydrothermal, solvothermal, hydrogen plasma-metal reaction, sol-gel, sonochemical and laser pyrolysis. They were utilized to synthesize nanostructures like nanorods, nanoflower, nanosphere, rose-like flowers, flower-like nanosheets, flowers of hexaogonal prism, nanodisc and micro-flower composed of spikes [6-23]. Hydrothermal method is one of the simple, efficient, cost effective methods to obtain rich morphologies of ZnO nanostructures and different mechanism have been proposed [24]. Research works have been focused on the construction of nanorods, sphere, flower-composed of rods, nanosheets etc [25-27]. Yao group reported the synthesis of FTO-coated ZnO micro sheets transformed to ZnO nanorods arrays by hydrogenation [28]. Sung Ho Kim et al., reported the synthesis of nanostructures of the sphere-like morphology using a template with amino acid [29]. Liu et al., reported tartaric acid assisted hydrothermal synthesis of different flower-like ZnO hierarchical architectures and tuned the optical properties by oxygen vacancies [30]. Jia et al. reported hierarchical ZnO sphere composed of dandelion by hydrothermal method [31]. Han et al. synthesized self-assembly nanorods of flower - like architectures with the assistance of HMTA (Hexamethylenetetramine) by hydrothermal method [32].These researchers used a template and other organic materials to prepare the ZnO nanostructure.

In this research, we have demonstrated a simple one pot hydrothermal method to synthesize ZnO nanoparticle, nanosheet, and nanorods in the absence of any organic capping agent and without annealing treatment in the atmosphere. The transformation process of ZnO morphology by NaOH at different temperature was discussed. Moreover, ZnO nanostructures was synthesized by adjusting the concentration of the NaOH precursor. The optical properties of ZnO were controlled by simply modifying the morphology of ZnO. The gas sensing response towards acetaldehyde was investigated.

2. Materials and Methods

Zinc nitrate [$Zn(NO_3)_2.6H_2O$] and Sodium hydroxide [NaOH] were purchased from Merck India and used without further purification.

2.1 Synthesis of ZnO nanostructures and fabrication of sensor device

In the typical synthesis, 0.1 mol $Zn(NO_3)_2.6H_2O$ was dissolved in 25 mL of deionized water and 0.05 mol of NaOH was dissolved in 5 mL of deionized water separately and both the solutions were stirred well for 1 h. The solution was transferred into 50 mL capacity Teflon-lined autoclave and kept at 200° C in a furnace for 5 h. After this process, the autoclave was cooled to room temperature. The white precipitate was centrifuged and washed several times with deionized water and ethanol, then dried at 60° C in hot air oven for 6 h. The above process was repeated with different concentration of NaOH while the concentrations of $Zn(NO_3)_2.6H_2O$ was kept constant. Different molar ratio of ($Zn(NO_3)_2.6H_2O$ and NaOH were used to synthesize ZnO nanocrystal. The samples are termed as S1 (0.1: 0.05), S2 (0.1: 0.1), S3 (0.1: 0.15) and S4 (0.1: 0.2).

Initially, 10 mg of ZnO powder was dissolved in 5 mL of ethanol and sonicated for 15 mins. Then, the colloidal solution was drop casted on gold interdigitated electrodes on quartz substrates. Finally, the prepared ZnO coated electrodes were dried in over for 1 h in 80^oC. The final sensing element schematic is shown in fig.1 a.

2.2 Characterization of different ZnO nanostructures

The X-ray diffraction (XRD) of the product was analyzed using X'per PRO (PANalytical) advanced X-ray Diffractometer with CuKα radiation (λ=1.5406 Å), with 2θ ranging between 20° and 80° at the scanning rate of 0.025° per second to determine the crystalline structure. The microstructure of the products was observed by QUANTA FEG field-emission scanning electron microscopy (FESEM) and Transmission electron microscope (TEM: JEOL JEM 2100F) at an accelerating voltage of 15 and 200 kV, respectively. Energy Dispersive X-ray analysis (EDX) was carried out. Raman spectra (Raman) were obtained using JASCO NR 1800 Raman spectrometer equipped with Nd : YAG laser. Optical properties were measured using Perkin Elmer Lambda 5 UV–Visible spectrophotometer and JASCO FB-8700 fluorescence spectrophotometer with excitation at 280 nm. Sensing responses were investigated using custom made gas testing chamber along with an electrometer (Fluke 8846A, USA). Photoluminescence

3. Result and Discussion:

3.1 Structural and morphological analysis of different ZnO nanostructures

XRD patterns of ZnO nano structures synthesized using different molar concentrations are shown in fig.1 b . The diffraction peaks for all the samples (S1, S2,S3, S4) corresponded to the wurtzite ZnO crystal structure (JCPDS card no.36 - 1451) [33]. No other impurities were observed from the patterns and the sharp peaks indicated that the ZnO nanostructures were crystalline nature. EDX analysis in fig.2 indicated that there were no impurities found in the particles. The morphology of ZnO nanoparticles was studied by FESEM. As depicted in fig. 3 it was clearly illustrated that the morphology of synthesized ZnO nanostructures depended on the NaOH molar concentration. NaOH acts as precursor as well as capping agent which modified the morphology of ZnO like nanoparticle, nanosheets, nanoflower and nano rods. The formation mechanism of the ZnO morphology of nanosheets and nano rods can be justified with NaOH concentration. Moreover, the relative concentration of Zn^{2+} of OH^- ions are very important.

$$Zn^{2+} + 2\ OH^- \longrightarrow Zn(OH)_2 \quad (1)$$

$$Zn(OH)_2 + 2\ OH^- \longrightarrow Zn(OH)_4^{2-} \quad (2)$$

$$Zn(OH)_4^{2-} \longrightarrow ZnO + H_2O + 2\ OH^- \quad (3)$$

The white precipitate $Zn(OH)_2$ was formed by addition of OH^- into Zn^{2+} contained solution. Further, increase in OH^- concentration leads to homogeneous solution of $Zn(OH)_4^{2-}$, which undergoes dehydration and forms ZnO nuclei. The growth of ZnO crystal is dominated by two polar planes like positive and negative planes terminated by Zn (0001) and by O $(000\bar{1})$. Zn (0001) plane is more active compared to other planes due to its high surface energy. This effect leads to formation of ZnO crystal growth in (0001) plane along c-axis. Hence, at the higher concentration of Zn^{2+} compared to OH^- concentration, the low OH^- concentration was taken place and there was no morphology change. However, when the excess concentration of OH^- ions compared to Zn^{2+} ions exists, the OH^- ions act as a caping agent [16-19]. It can lead to the growth of ZnO nanoparticles along the C_2 axis and form the nanorods- like structure [34].

FESEM image of sample S1 (1:0.05 molar ratio Zinc nitrate: NaOH) showed nanoparticles-like morphology was formed as observed in fig. 4 (a). ZnO nanosheet-like morphology was observed with sample S2 (1:1 molar ratio Zinc nitrate: NaOH) as precursor concentration increased and the nanosheets with different shape and size were seen (fig.4 b). Some of the nanosheets were hexagonal in shape. However, from the fig. 4c, both nanosheets

and nanorods morphology were observed in the sample S3. Thus, it is also evident that the morphology of ZnO nanostructures was influenced by the concentration of OH^- ions. Moreover, the sample S4 (1:2 molar ratio) with higher concentration of precursor showed nanorods-like morphology (Fig.4 d) was formed. It might be due to the excess concentration of OH^- ions. It was seen that the tetragonal morphology was formed at the edge of the nanorods. TEM and HRTEM images of the ZnO nanostructure S3 and S4 are depicted in the fig.5. The hexagonal-like nanosheets and nanorods morphology were clearly seen. The clear and uniform lattice fringes in the HR-TEM image confirmed that the nanorods and nanosheets were well crystalline. Liu.et al., reported similar growth of nanorods with different molar ratio of Zn^{2+} to Na_2O_2 [30].

3.2. Optical properties, chemical bonding and XPS analysis

Fig.6 shows the FTIR spectra of ZnO nanostructures (S1, S2, S3, S4). The broad absorption band at 3404 cm^{-1} ascribed to the O-H bending vibration of water molecules absorbed on the ZnO nanostructures. The vibration at 1623 cm^{-1} corresponded to the O-H vibration [35, 36]. The peak at 871 cm^{-1} corresponded to the formation of tetrahedral coordination of Zn. The sharp peak at 556 cm^{-1} was ascribed to the Zn-O [37-40]. The UV-visible absorption spectra for different ZnO nanostructure are shown in fig 7. All the samples exhibited single absorption band and the position of peak depend on the ZnO shape and size of samples. The decrease in the dimension and particle size constrains the electrons and holes and thus leads to shift in the absorption edge towards lower wavelength [41]. The absorption edge of nanoparticles, nanosheets, a mixture of nanosheets-rods and nanorods (S1, S2, S3, S4) were 382, 380, 378 and 376 nm, respectively. All the samples exhibited the slight blue shift. Since the Bohr exciton radius of ZnO is very small, the blue shift cannot correspond to quantum effect. It may be might be coupling effect among the particles [41].

The Raman spectra of ZnO samples S1, S2, S3 and S4 at room temperature are shown in fig. 8. The peak at 438 cm^{-1} was due to non-optical phonon E_{2H} mode. It confirmed the wurtzite structure of ZnO nanostructures [42]. Moreover, the weak peaks at 330 cm^{-1} and 380 cm^{-1} ascribed to multi – phonons scattering process E_{2H} - E_{2L} and A1 phonons, respectively. Compared to ZnO nanoparticles and nanosheets (S1 and S2), the ZnO nanorods (S4) had a higher intensity peak at 580 cm^{-1}. This can be justified due to the presence of higher interstitial zinc and oxygen vacancy on the surface of ZnO [43]. Fig. 9 shows the PL spectra of different nanostructures. The sample S1 showed a peak at 370 nm whereas samples S2, S3 and S4

showed a peak at 375 nm. It is attributed the near–band edge emission resulting from the band edge transition or recombination of excitons [41, 44, 45]. The sharp UV emission peak arised due to recombination of exciton bound to neutral donor or acceptors. The low intense peaks at 434, 500 nm (blue – green emission) were due to the intrinsic vacancy of zinc, oxygen vacancy and surface defects. [41, 46]. The broading in blue-green emission corresponded to phonon-assisted transition. However, compared to nanoparticles, the peak intensity of nanosheets and nanorods were higher. Thus, the morphology of nanostructures can influence the photoluminescence intensity [47].

XPS spectra of ZnO nanorods (S4) shown in fig. 10 a displayed two peaks centered at 1022.47 and 1045.50 eV, corresponding to Zn $2p_{3/2}$ and Zn $2p_{1/2}$, respectively. The peak at 1022.47 eV specified that the Zn was coordinated or bonded to other elements (elemental Zn: 1020 eV) [48]. The O 1s peak positioned at the lower binding energy of 530.8 eV (fig. 10 b), was assigned to O^{2-} ions in the Zn–O bonding of the wurtzite structure of ZnO. The peak located at 532.3 eV was related to OH group absorbed onto the surface of the ZnO nanorods [49].

3.3 Gas sensing analysis and mechanism

The sensing responses were calculated using the relationship $S = R_a/R_g$. Where R_a is the resistance in air and R_g is the resistance in test gas atmosphere. The sample was exposed towards different gases like ethanol, methanol, acetaldehyde and toluene as shown in Fig. 11 a. ZnO nanorods showed good response towards acetaldehyde compared with other gases. Initially the sensing nature of all four different nanostructures was tested towards fixed concentration of acetaldehyde. Fig. 11 b shows the sensing response towards 100 ppm of acetaldehyde for nanoparticles (S1), nanosheets (S2), nanoflowers (S3) and nanorods (S4). The response values were 1.5, 3.9, 9.6 and 91 for S1, S2, S3 and S4, respectively. ZnO nanorods (S4) exhibited higher sensitivity than other three nanostructures. To further elucidate the sensor responses, various concentrations of acetaldehyde were exposed to nanorods. The observed concentration vs response is shown in Fig. 11 c. As the concentration increased the sensing response also increased. It indicated that proper redox reactions occur during solid gas interaction even at high concentrations i.e. 500 ppm. Fig. 11 d shows the single transient resistance response for 200 ppm of acetaldehyde. For 200 ppm of concentration, response and recovery times were 40 and 80 s respectively.

Based on the experimental investigation, gas sensing mechanism is proposed. When n-type ZnO was exposed to ambient atmosphere, the atmospheric oxygen trapped the surface

electrons of ZnO which resulted in creating space charge region. Likewise, when the chamber loaded with target gas, these molecules react with pre-adsorbed oxygen ions. By removing pre-adsorbed oxygen ions, trapped electrons put back into ZnO which leads to decrease in surface resistance. The increase in conductivity can be well understood by percolative threshold of electrons through grains with increasing gas concentration [50-53].

The possible sensing mechanism [54,55] on ZnO nanorods is given in eqn. 4 and 5,

$$O_{2\,(atmosphere)} + e^{-}_{(ZnO\ surface)} \longrightarrow O^{-}_{2\,(ZnO\ surface)} \quad \text{------- (4)}$$

$$2CH_3CHO + 5O_2^{-}{}_{(ZnO\ surface)} \longrightarrow 4CO_2 \uparrow + 4H_2O \uparrow + 5e^{-}{}_{(ZnO\ surface)} \quad \text{------- (5)}$$

The release of CO_2 during interaction with ZnO surface is already proved by lime water test in our previous works [4]. The selectivity of the nanorods (S4) was investigated towards 100 ppm of interfering gases such as ethanol, methanol and toluene. No interference was observed with other vapors and the sensor showed good stability over a period of 15 days. The probable reason for the high selectivity is lower bond dissociation energy of acetaldehyde (364 kJ mol^{-1}) than ammonia (435 kJ mol^{-1}), ethanol (436 kJ mol^{-1}), methanol (436.8 kJ mol^{-1}) and toluene (368 kJ mol^{-1}) [54-55].

4. Conclusion

ZnO hierarchical nanostructures were successfully synthesized by one step hydrothermal process without any additives and capping agents. Morphology of ZnO was modified using NaOH self-capping agent, which had no toxicity when compared to organic capping agents. FESEM clearly revealed that the particles were transformed from nanoparticles to nanorods. PL spectra showed that ZnO nanorods consisted of higher Zinc and oxygen defect compared to other samples. ZnO nanorods showed higher gas response of S = 91 towards acetaldehyde. It also showed good stability at higher concentration of about 500 ppm.

Acknowledgements

This work was financially supported by Research Institute of Electronics, Shizuoka University. We also thank Prof. K. Murakami, Mr. T. Koyama and Mr. W. Tomoda, Center for Nanodevices fabrication and analysis for instrumental facilities. R. Sankar Ganesh would like to thank MEXT japan for the award of MEXT fellowship.

5. Reference

[1] A. Loutfi, S. Coradeschi, G.K. Mani, P. Shankar, J.B.B. Rayappan, Electronic noses for food quality: A review, J. Food Eng. 144 (2015) 103–111. doi:10.1016/j.jfoodeng.2014.07.019.

[2] P. Shankar, J.B.B. Rayappan, Gas sensing mechanism of metal oxides: The role of ambient atmosphere, type of semiconductor and gases - A review, Sci. Lett. 4 (2015) 126 (1-18).

[3] H. Jiang, J. Hu, F. Gu, C. Li, Template-free approach for hydrothermal fabrication of ZnO microspheres, Particuology, 7 (2009) 225–228. doi:10.1016/j.partic.2009.01.010.

[4] R. Sankar Ganesh, M. Navaneethan, G.K. Mani, S. Ponnusamy, K. Tsuchiya, C. Muthamizhchelvan, S. Kawasaki, Y. Hayakawa, Influence of Al doping on the structural, morphological, optical, and gas sensing properties of ZnO nanorods, J. Alloys Compd. (2017). doi:10.1016/j.jallcom.2016.12.187.

[5] A. Umar, M.S. Chauhan, S. Chauhan, R. Kumar, G. Kumar, S.A. Al-sayari, S.W. Hwang, A. Al-hajry, Large-scale synthesis of ZnO balls made of fluffy thin nanosheets by simple solution process: Structural, optical and photocatalytic properties, J. Colloid Interface Sci. 363 (2011) 521–528. doi:10.1016/j.jcis.2011.07.058.

[6] Q. Ding, Y. Miao, T. Liu, Morphology and photocatalytic property of hierarchical polyimide/ZnO fibers prepared via a direct ion-exchange process, (2013). doi:10.1021/am4009488.

[7] K.P. Ghoderao, S.N. Jamble, R.B. Kale, Optik Influence of pH on hydrothermally derived ZnO nanostructures, Opt. - Int. J. Light Electron Opt. 156 (2018) 758–771. doi:10.1016/j.ijleo.2017.10.046.

[8] F.H. Alsultany, Z. Hassan, N.M. Ahmed, N.G. Elafadill, H.R. Abd, Effects of ZnO seed layer thickness on catalyst-free growth of ZnO nanostructures for enhanced UV photoresponse, Opt. Laser Technol. 98 (2018) 344–353. doi:10.1016/j.optlastec.2017.06.031.

[9] J. Yang, H. Jia, X. Lv, Y. Wang, Facile preparation of urchin-like ZnO nanostructures and their photocatalytic performance, Ceram. Int. 42 (2016) 12409–12413. doi:10.1016/j.ceramint.2016.04.180.

[10] M. Tan, J. Kim, M. Seok, A.T. Do, H. Seok, Oriented ZnO nanostructures and their application in photocatalysis, J. Lumin. 185 (2017) 17–22. doi:10.1016/j.jlumin.2016.12.046.

[11] M.P. Navas, R.K. Soni, N. Tarasenka, N. Tarasenko, Applied Surface Science Temperature and solution assisted synthesis of anisotropic ZnO nanostructures by pulsed laser ablation, Appl. Surf. Sci. 414 (2017) 413–423. doi:10.1016/j.apsusc.2017.04.091.

[12] L. Zhu, W. Zeng, A novel coral rock-like ZnO and its gas sensing, Mater. Lett. 209 (2017) 244–246. doi:10.1016/j.matlet.2017.08.020.

[13] M.A. Alvi, A.A. Al-ghamdi, M. Shaheerakhtar, Synthesis of ZnO nanostructures via low temperature solution process for photocatalytic degradation of rhodamine B dye, Mater. Lett. 204 (2017) 12–15. doi:10.1016/j.matlet.2017.06.005.

[14] A. Tavakoli, M. Sohrabi, A. Kargari, REVIEW A Review of Methods for Synthesis of Nanostructured Metals with Emphasis on Iron Compounds, Chem. Pap. 61 (2007) 151–170. doi:10.2478/s11696-007-0014-7.

[15] J.N. Hasnidawani, H.N. Azlina, H. Norita, N.N. Bonnia, Synthesis of ZnO Nanostructures Using Sol-Gel Method, Procedia Chem. 19 (2016) 211–216. doi:10.1016/j.proche.2016.03.095.

[16] D. Yolaçan, N. Demirci, Enhanced photoelectrochemical and photocatalytic properties of 3D- hierarchical ZnO nanostructures, J. Alloys Compd. 726 (2017) 474–483. doi:10.1016/j.jallcom.2017.07.314.

[17] M. Taheri, H. Abdizadeh, M. Reza, Formation of urchin-like ZnO nanostructures by sol-gel electrophoretic deposition for photocatalytic application, J. Alloys Compd. 725 (2017) 291–301. doi:10.1016/j.jallcom.2017.07.173.

[18] L. Lin, J. Liu, J. Lv, S. Shen, X. Wu, Correlation between native defects and morphological , structural and optical properties of ZnO nanostructures, J. Alloys Compd. 695 (2017) 1523–1527. doi:10.1016/j.jallcom.2016.10.292.

[19] R. Agung, F. Hermann-westendorf, A. Dellith, C. Schmidt, J. Dellith, J. Plentz, M. Schulz, M. Presselt, M. Seyring, M. Rettenmeyer, B. Dietzek, Effect of annealing on the sub-bandgap , defects and trapping states of ZnO nanostructures, Chem. Phys. 483–484 (2017) 112–121. doi:10.1016/j.chemphys.2016.12.002.

[20] X. Lv, X. Liu, Q. Sun, Y. Wang, B. Yan, Growth and optical properties of hierarchical fl ower-like ZnO nanostructures, Ceram. Int. 43 (2017) 3306–3313. doi:10.1016/j.ceramint.2016.11.168.

[21] A.U. Badnore, A.B. Pandit, E ff ect of pH on sonication assisted synthesis of ZnO nanostructures : Process details, Chem. Eng. Process. Process Intensifi Cation. 122 (2017) 235–244. doi:10.1016/j.cep.2017.09.013.

[22] L. Zhu, Y. Li, W. Zeng, Applied Surface Science Hydrothermal synthesis of hierarchical flower-like ZnO nanostructure and its enhanced ethanol gas-sensing properties, Appl. Surf. Sci. 427 (2018) 281–287. doi:10.1016/j.apsusc.2017.08.229.

[23] A.O. Dikovska, D. Pallotti, S. Lettieri, G.B. Atanasova, G. V Avdeev, P. Maddalena, S. Amoruso, N.N. Nedyalkov, Applied Surface Science Growth mechanism of ZnO nanostructures produced by ultraviolet and visible laser ablation, Appl. Surf. Sci. 423 (2017) 977–982. doi:10.1016/j.apsusc.2017.06.331.

[24] T. Sio, L. Zhang, X. Li, Z. Chang, D. Li, Preparation , characterization and photoactivity of hollow N , Co, TiO2/SiO2 microspheres, Materials Sci. Semi. Process. 214 (2011) 52–57. doi:10.1016/j.mssp.2011.01.004.

[25] L. Fang, B. Zhang, W. Li, X. Li, T. Xin, Controllable synthesis of ZnO hierarchical architectures and their photocatalytic property, Superlattices Microstruct. 75 (2014) 324–333. doi:10.1016/j.spmi.2014.03.001.

[26] X. Fang, Y. Li, S. Zhang, L. Bai, N. Yuan, J. Ding, The dye adsorption optimization of ZnO nanorod-based dye-sensitized solar cells, Sol. Energy. 105 (2014) 14–19. doi:10.1016/j.solener.2014.03.039.

[27] H. Zhang, C. Xu, P. Sheng, Y. Chen, L. Yu, Q. Li, Synthesis of ZnO hollow spheres through a bacterial template method and their gas sensing properties, Sen. Actuators B. Chem. 181 (2013) 99–103. doi:10.1016/j.snb.2013.01.002.

[28] C. Yao, B. Wei, H. Ma, L. Meng, X. Zhang, Q. Gong, Enhanced photoelectrochemical performance of hydrogenated ZnO hierarchical nanorod arrays, J. Power Sources. 237 (2013) 295–299. doi:10.1016/j.jpowsour.2013.02.062.

[29] S.H. Kim, T.Y. Olson, J.H.S. Jr, T.Y. Han, Hierarchical ZnO structures templated with amino acid based surfactants, Microporous Mesoporous Mater. 151 (2012) 64–69. doi:10.1016/j.micromeso.2011.11.015.

[30] T. Liu, Y. Li, H. Zhang, M. Wang, X. Fei, S. Duo, Y. Chen, J. Pan, W. Wang, Tartaric acid assisted hydrothermal synthesis of different flower-like ZnO hierarchical architectures with tunable optical and oxygen vacancy-induced photocatalytic properties, Appl. Surf. Sci. 357 (2015) 516–529.

[31] Q. Jia, H. Ji, Y. Zhang, Y. Chen, X. Sun, Z. Jin, Rapid and selective detection of acetone using hierarchical zno gas sensor for hazardous odor markers application, J. Hazard. Mater. 276 (2014) 262–270. doi:10.1016/j.jhazmat.2014.05.044.

[32] Z. Han, L. Liao, Y. Wu, H. Pan, S. Shen, J. Chen, Synthesis and photocatalytic application of oriented hierarchical ZnO flower-rod architectures, J. Hazard. Mater. 217–218 (2012) 100–106. doi:10.1016/j.jhazmat.2012.02.074.

[33] G. Lu, X. Wang, J. Liu, S. Qiu, C. He, B. Li, W. Liu, One-pot synthesis and gas sensing properties of ZnO mesoporous architectures, Sensors Actuators, B Chem. 184 (2013) 85–92. doi:10.1016/j.snb.2013.04.075.

[34] M.R. Alenezi, S.J. Henley, G. Emerson, S.R.P. Silva, From 1D and 2D ZnO nanostructures to 3D Hierarchical structures with enhanced gas sensing properties, Nanoscale, (2014), 235–247. doi:10.1039/c3nr04519f.

[35] G. Hitkari, S. Singh, G. Pandey, Nano-Structures & Nano-Objects Structural , optical and photocatalytic study of ZnO and ZnO – ZnS synthesized by chemical method, Nano-Structures & Nano-Objects. 12 (2017) 1–9. doi:10.1016/j.nanoso.2017.08.007.

[36] R.N. Gayen, R. Paul, Nano-Structures & Nano-Objects Phosphorous doping in vertically aligned ZnO nanorods grown by wet-chemical method, Nano-Structures & Nano-Objects. 13 (2018) 163–169. doi:10.1016/j.nanoso.2016.03.007.

[37] M. Gharagozlou, S. Naghibi, Sensitization of ZnO nanoparticle by vitamin B 12 : Investigation of microstructure , FTIR and optical properties, Mater. Res. Bull. 84 (2016) 71–78. doi:10.1016/j.materresbull.2016.07.029.

[38] S. Ameen, M.S. Akhtar, H. Shik, Growth and characterization of nanospikes decorated ZnO sheets and their solar cell application, Chem. Eng. J. 195–196 (2012) 307–313. doi:10.1016/j.cej.2012.04.081.

[39] J. Qin, X. Zhang, Y. Xue, N. Kittiwattanothai, A facile synthesis of nanorods of ZnO/ graphene oxide composites with enhanced photocatalytic activity, Appl. Surf. Sci. 321 (2014) 226–232. doi:10.1016/j.apsusc.2014.10.008.

[40] R.Y. Hong, J.H. Li, L.L. Chen, D.Q. Liu, H.Z. Li, Y. Zheng, J. Ding, Synthesis , surface modification and photocatalytic property of ZnO nanoparticles, Powder Technol. 189 (2009) 426–432. doi:10.1016/j.powtec.2008.07.004.

[41] M. Ramani, S. Ponnusamy, C. Muthamizhchelvan, From zinc oxide nanoparticles to microflowers: A study of growth kinetics and biocidal activity, Mater. Sci. Eng. C. 32 (2012) 2381–2389. doi:10.1016/j.msec.2012.07.011.

[42] M. Navaneethan, J. Archana, M. Arivanandhan, Y. Hayakawa, Functional properties of amine-passivated ZnO nanostructures and dye-sensitized solar cell characteristics, Chem. Eng. J. 213 (2012) 70–77. doi:10.1016/j.cej.2012.10.001.

[43] J.C. Sin, S.M. Lam, K.T. Lee, A.R. Mohamed, Self-assembly fabrication of ZnO hierarchical micro/nanospheres for enhanced photocatalytic degradation of endocrine-disrupting chemicals, Mater. Sci. Semicond. Process. 16 (2013) 1542–1550. doi:10.1016/j.mssp.2013.05.008.

[44] J. Zhao, L. Wang, X. Yan, Y. Yang, Y. Lei, J. Zhou, Y. Huang, Y. Gu, Y. Zhang, Structure and photocatalytic activity of Ni-doped ZnO nanorods, Mater. Res. Bull. 46 (2011) 1207–1210. doi:10.1016/j.materresbull.2011.04.008.

[45] E. Marsili, Morphology-directed synthesis of ZnO nanostructures and their antibacterial activity, Colloids Surfaces B Biointerfaces. 105 (2013) 24–30. doi:10.1016/j.colsurfb.2012.12.056.

[46] S. Yue, J. Lu, J. Zhang, Controlled growth of well-aligned hierarchical ZnO arrays by a wet chemical method, Mater. Lett. 63 (2009) 2149–2152. doi:10.1016/j.matlet.2009.06.055.

[47] M. Mazhdi, J. Saydi, M. Karimi, J. Seidi, F. Mazhdi, A study on optical, photoluminescence and thermoluminescence properties of ZnO and Mn doped-ZnO nanocrystalline particles, Optik (Stuttg). 124 (2013) 4128–4133. doi:10.1016/j.ijleo.2012.12.068.

[48] R. Al-gaashani, S. Radiman, A.R. Daud, N. Tabet, Y. Al-douri, XPS and optical studies of different morphologies of ZnO nanostructures prepared by microwave methods, Ceram. Int. 39 (2013) 2283–2292. doi:10.1016/j.ceramint.2012.08.075.

[49] R.S. Ganesh, M. Navaneethan, V.L. Patil, S. Ponnusamy, C. Muthamizhchelvan, S. Kawasaki, P.S. Patil, Y. Hayakawa, Sensitivity enhancement of ammonia gas sensor based on Ag/ZnO flower and nanoellipsoids at low temperature, Sensors Actuators B. Chem. (2017). doi:10.1016/j.snb.2017.08.015.

[50] G.K. Mani, J.B.B. Rayappan, Novel and Facile Synthesis of Randomly Interconnected ZnO Nanoplatelets Using Spray Pyrolysis and Their Room Temperature Sensing Characteristics, Sensors Actuators B Chem. 198 (2014) 125–133. doi:10.1016/j.snb.2014.02.101.

[51] G.K. Mani, J.B.B. Rayappan, ZnO nanoarchitectures: Ultrahigh sensitive room temperature acetaldehyde sensor, Sensors Actuators B Chem. 223 (2016) 343–351. doi:10.1016/j.snb.2015.09.103.

[52] B. Vutukuri, G.K. Mani, P. Shankar, J.B.B. Rayappan, Thickness Dependent Room Temperature Sensing Properties of Spray Pyrolysis Deposited Nanostructured ZnO Thin Films Brahmaiah, Nanosci. Nanotechnol. Lett. 7 (2015) 885–891. doi:10.1166/jnn.2016.10643.

[53] K. Sivalingam, P. Shankar, G.K. Mani, J.B.B. Rayappan, Solvent volume driven ZnO nanopetals thin films Spray pyrolysis, Mater. Lett. 134 (2014) 47–50.

[54] P. Rai, Y.-T.T. Yu, Citrate-assisted hydrothermal synthesis of single crystalline ZnO nanoparticles for gas sensor application, Sensors Actuators B Chem. 173 (2012) 58–65. doi:10.1016/j.snb.2012.05.068.

[55] J. Xu, J. Han, Y. Zhang, Y. Sun, B. Xie, Studies on alcohol sensing mechanism of ZnO based gas sensors, Sensors Actuators B Chem. 132 (2008) 334–339. doi:10.1016/j.snb.2008.01.062.

Figures

Figures

Figure caption

Figure . 1 (a) Schematic of the sensing electrode, (b) XRD patterns of ZnO nanostructures.

Figure . 2 EDX analysis of S3 sample

Fig. 3 Growth mechanism of ZnO nanostructure

Fig . 4 FESEM images of ZnO nanostructures (a). S1, (b). S2, (c). S3 and (d). S4 sample, respectively.

Figure. 5 TEM and HRTEM image for ZnO nanostructures (a, b). S3, (c, d). S4 sample

Figure. 6 FTIR spectra of ZnO nanostructures.

Figure. 7 UV-vis absoption spectra of ZnO nanostructures.

Figure. 8 Raman spectra of ZnO nanostructures.

Figure. 9 PL spectra of ZnO nanostructures sample

Figure. 10 XPS analysis of ZnO nanorod

Figure. 11 a) Selectivity trend of S4 samples towards various interfering vapors (b) Response comparison with respect to four different nanostructures, c) response values with respect to various concentration from 2 to 500 ppm of acetaldehyde for S4 and d) single transient resistance response towards 200 ppm of acetaldehyde.

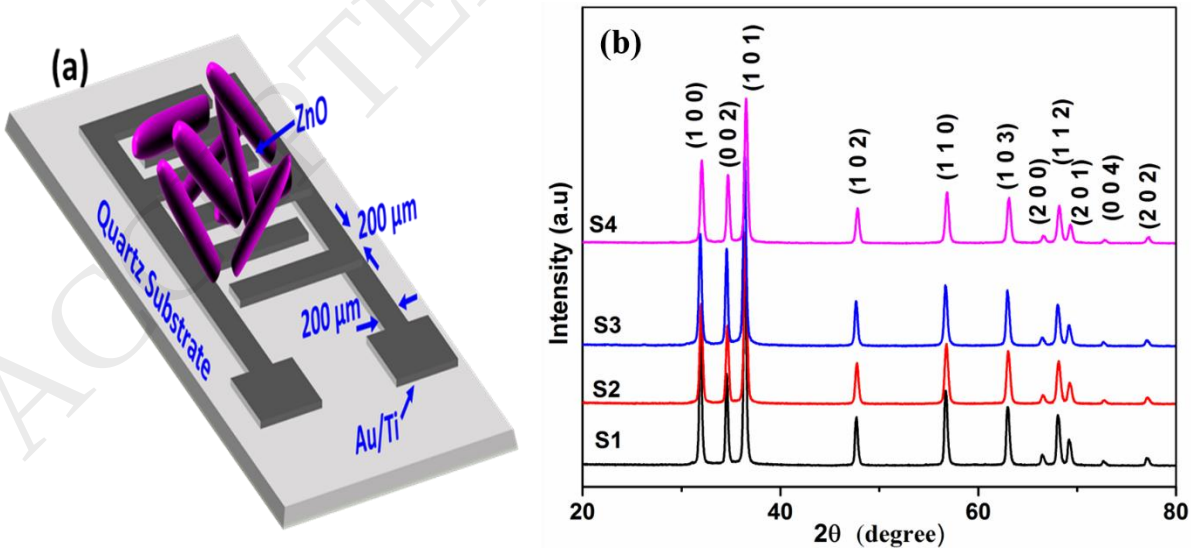

Figure 1

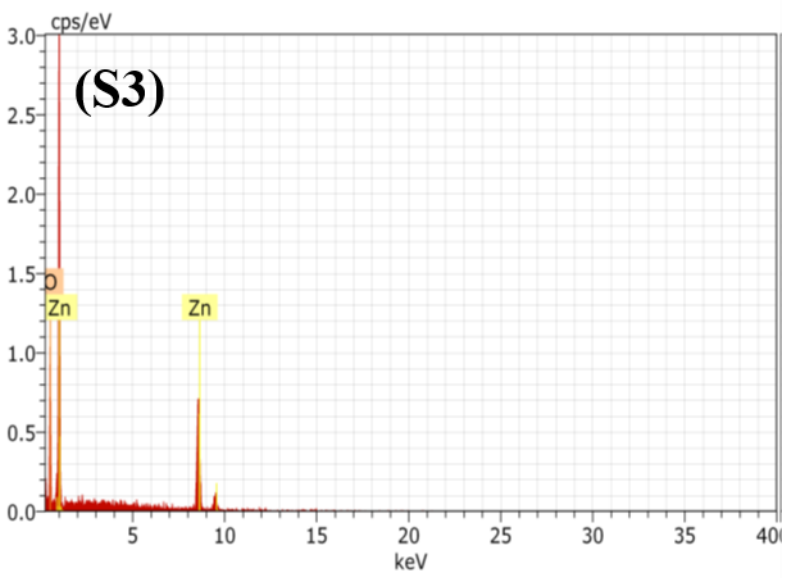

Figure 2

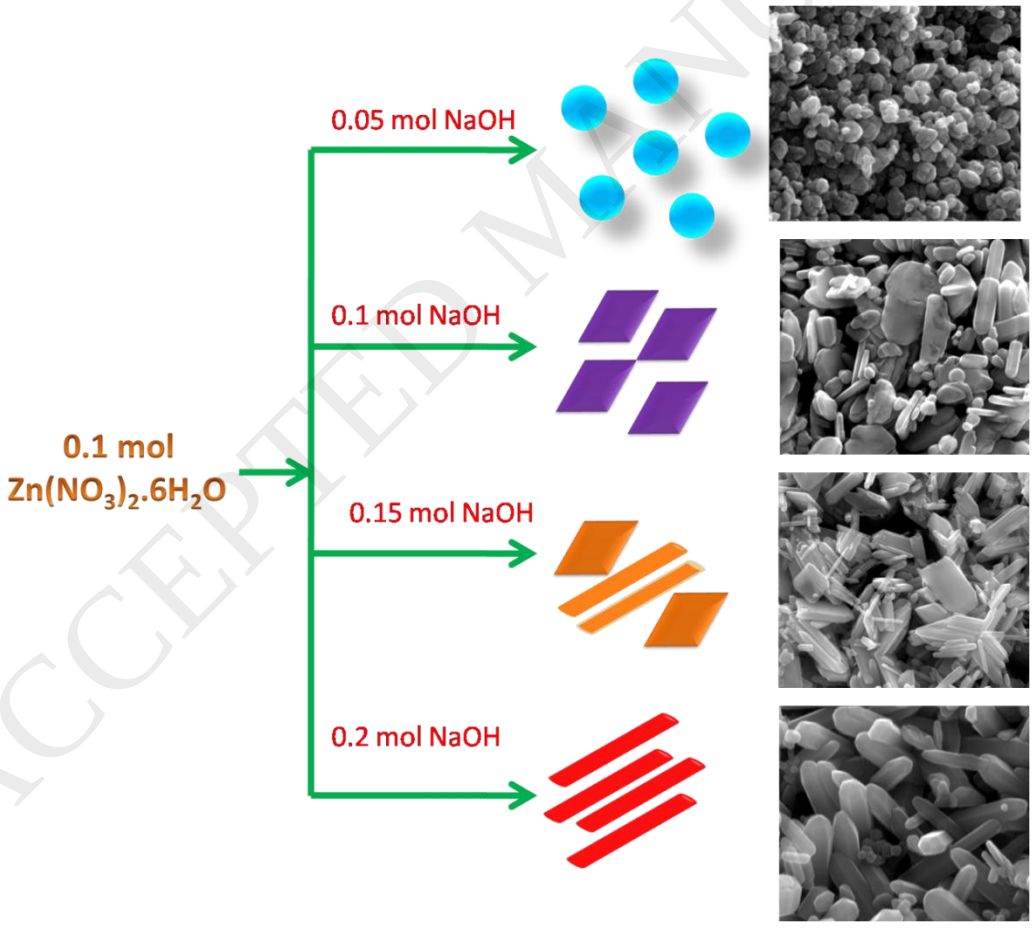

Figure 3

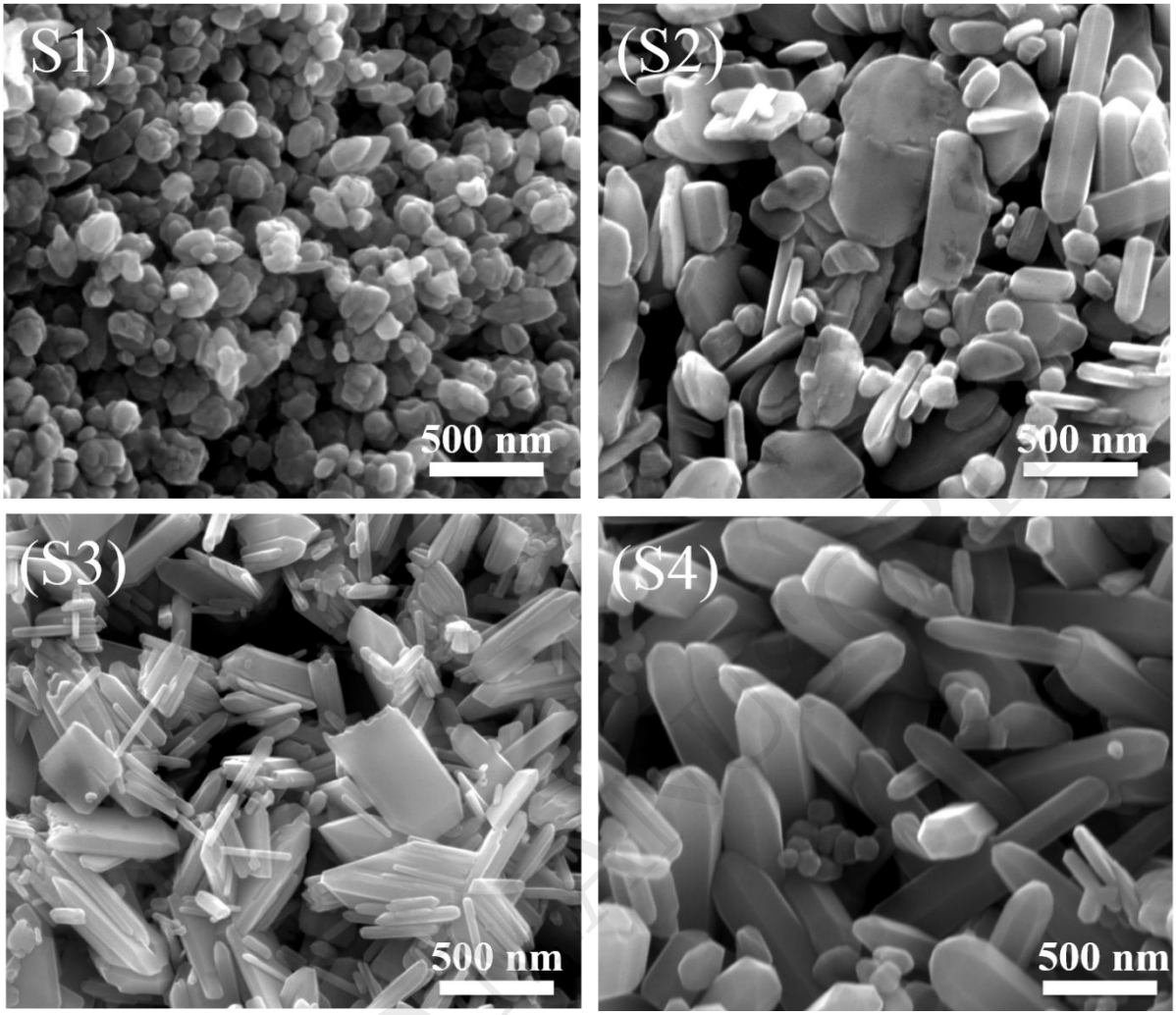

Figure 4

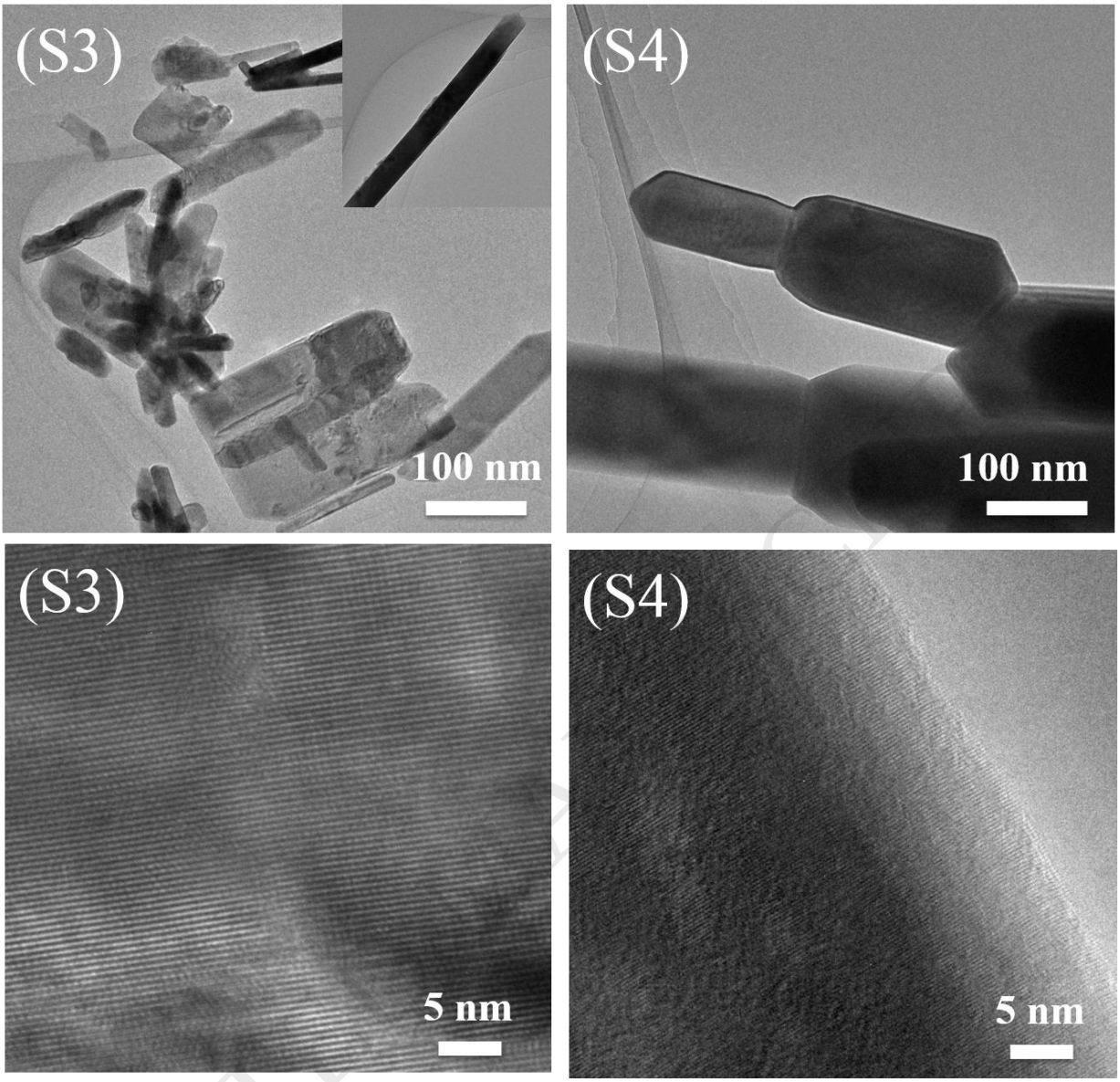

Figure 5

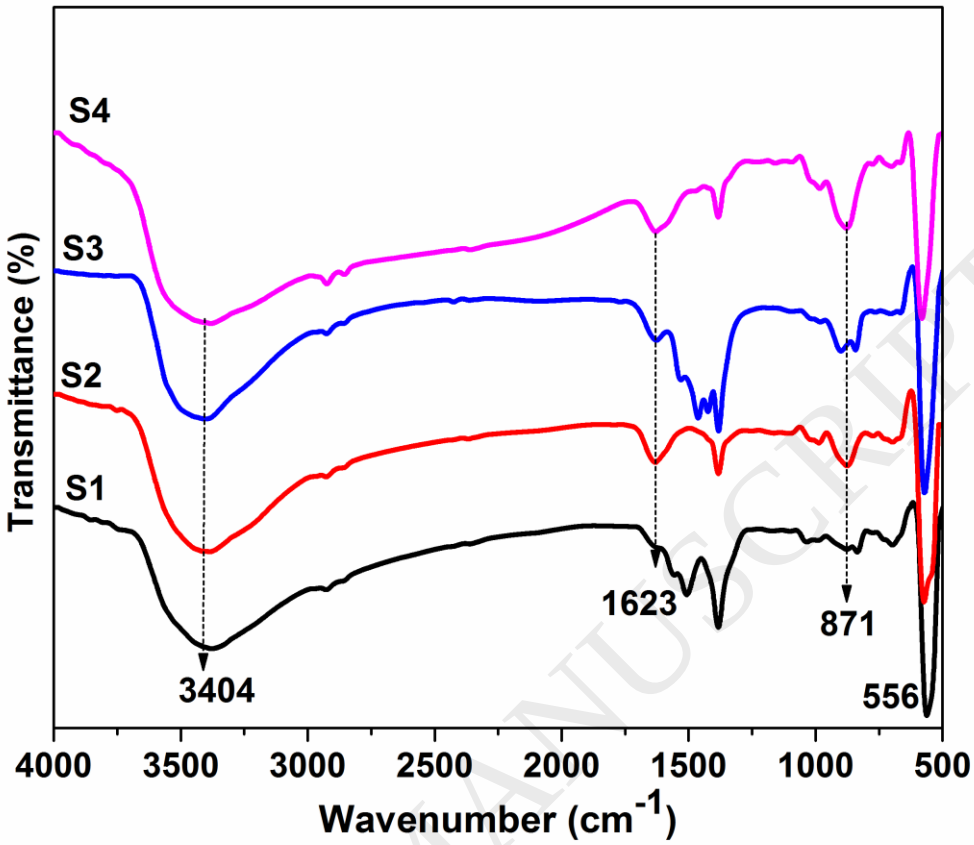

Figure 6

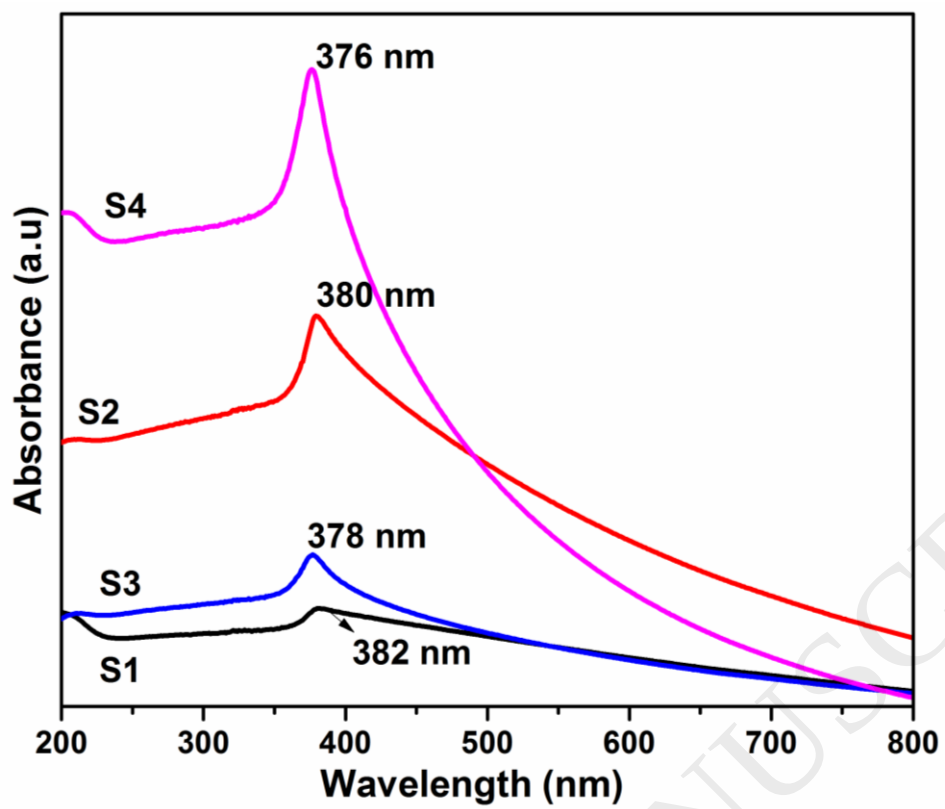

Figure 7

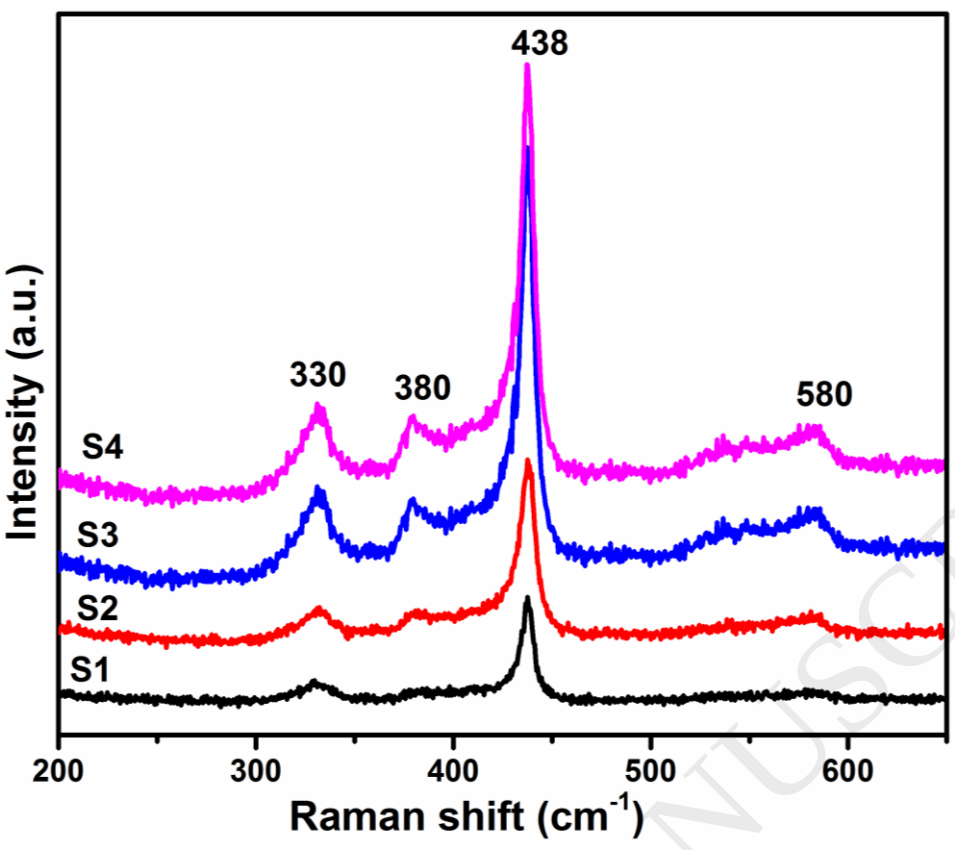

Figure 8

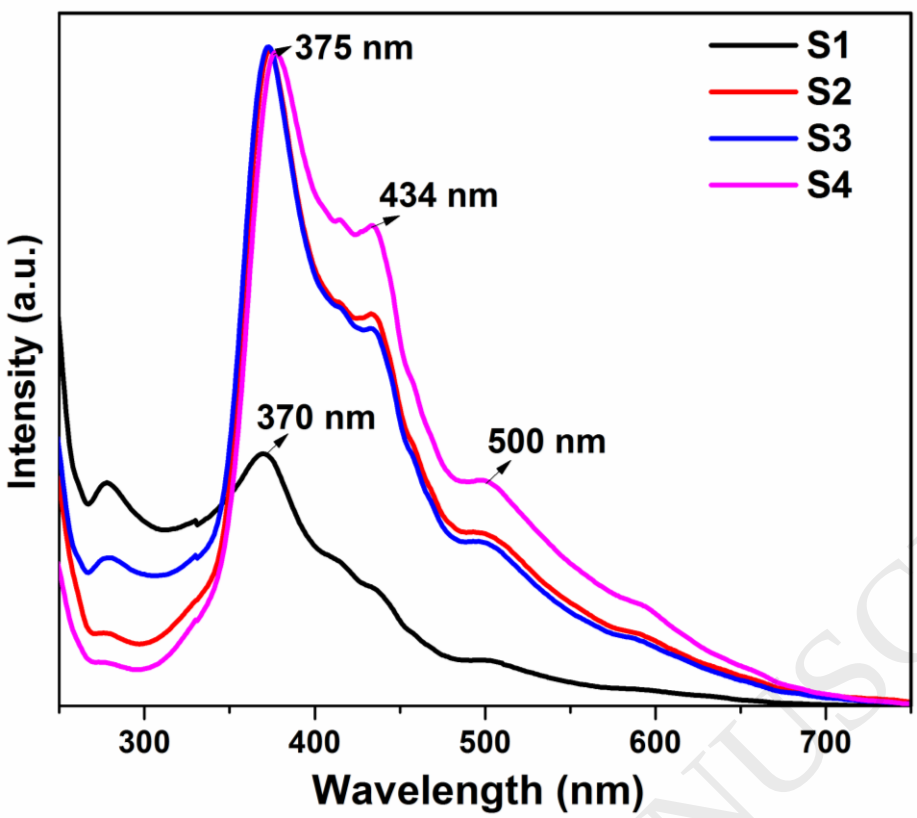

Figure 9

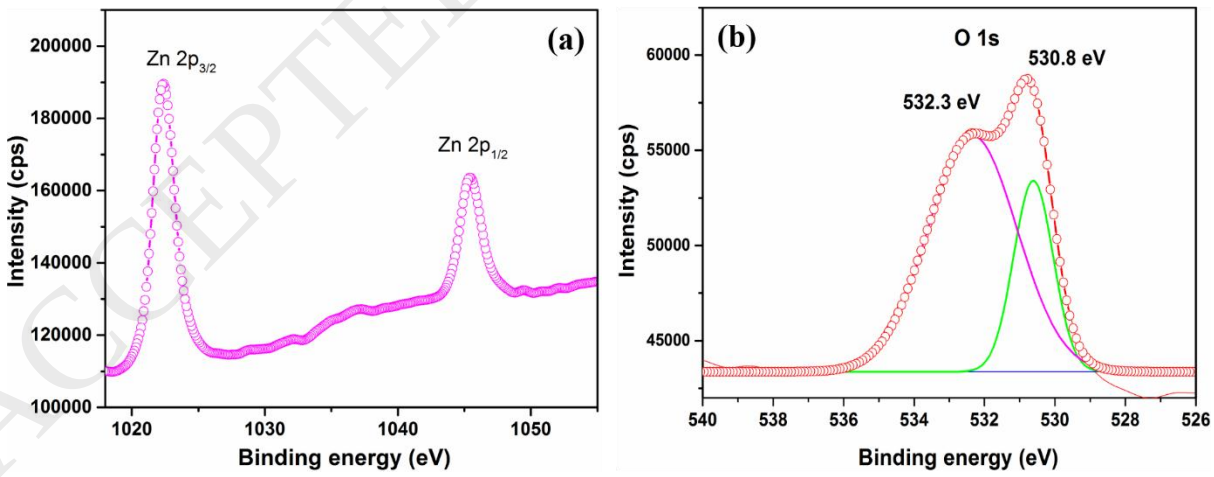

Figure 10

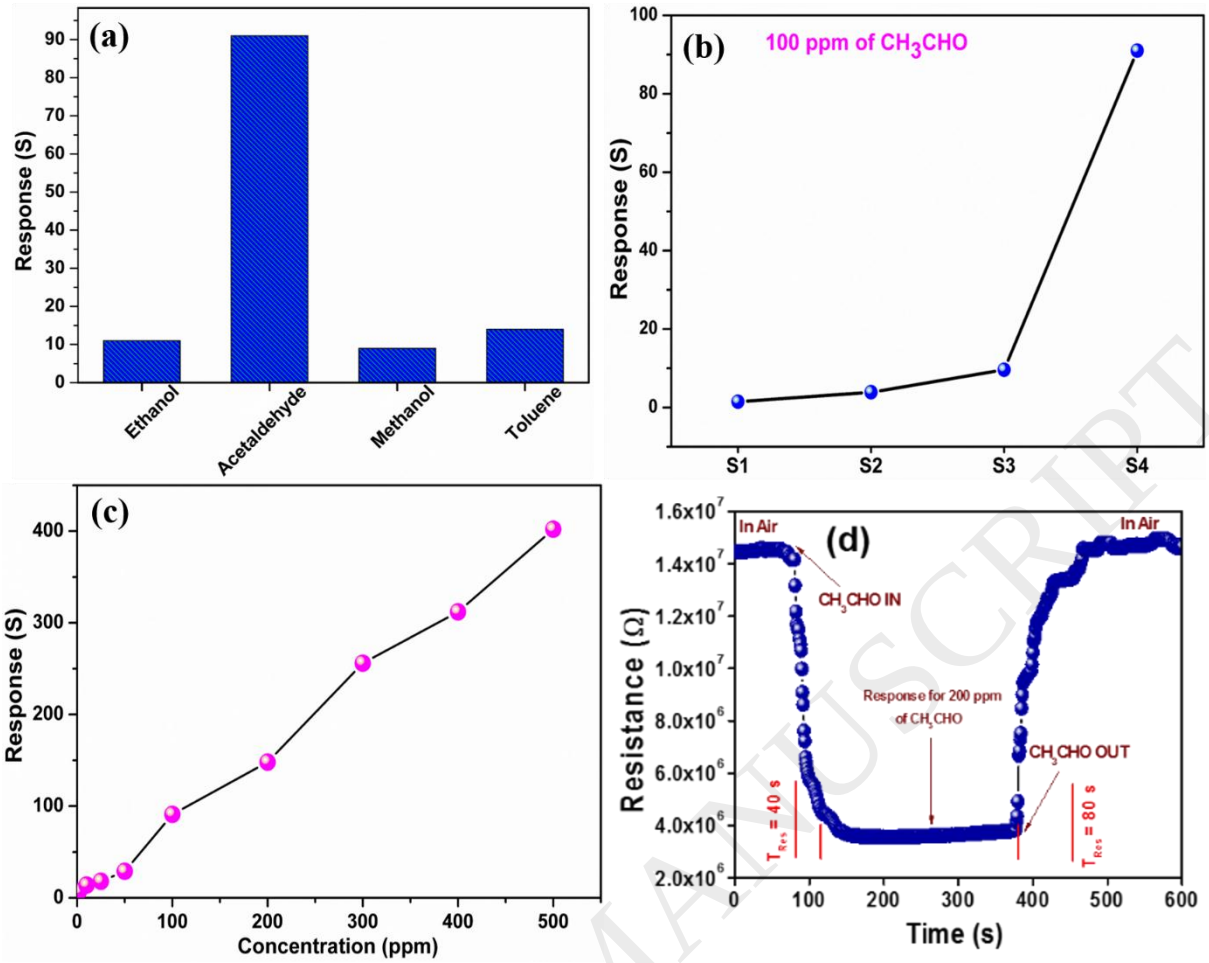

Figure 11